IEEE Access
Multidisciplinary ⋮ Rapid Review ⋮ Open Access Journal

Received 18 January 2024, accepted 26 February 2024, date of publication 7 March 2024, date of current version 13 March 2024.

Digital Object Identifier 10.1109/ACCESS.2024.3373695

RESEARCH ARTICLE

4WS Intelligent Fire-Fighting Robot Trajectory Tracking Control Based on Adaptive Cornering Stiffness

LIN ZHONG, XUDONG JIANG, WENLONG JIA, AND WEI SHI
Shanghai Fire Research Institute, Ministry of Emergency Management, Shanghai 200032, China
Corresponding author: Wei Shi (19505285267@163.com)

This work was supported in part by the National Key Research and Development Program of China under Grant 2020YFC1512101.

ABSTRACT To address the challenges posed by nonlinear tire characteristics in trajectory tracking control of active four-wheel steering (4WS) vehicle or fire-fighting robot, a novel control method is proposed. This method incorporates time-varying corrected cornering stiffness to enhance adaptability. Initially, the impact of friction coefficient and vertical load on tire lateral force nonlinearity is analyzed. Key input features are identified, and a cornering stiffness estimation model is developed using a Back Propagation (BP) neural network. Subsequently, the trajectory tracking state equation is established based on the 2-degree-of-freedom (2-DOF) dynamic model and trajectory tracking error model. An active front-wheel steering (AFS) trajectory tracking sliding mode controller (SMC) is designed, augmented by a Radial Basis Function (RBF) neural network, forming an RBF-SMC AFS controller capable of real-time correction of cornering stiffness. Additionally, an active rear-wheel steering (ARS) controller is designed based on fuzzy control theory, considering the influence of center of gravity lateral deviation on vehicle stability. Finally, Simulation tests under varied speed conditions on icy and dry asphalt surfaces, using the Matlab/Simulink-Carsim co-simulation platform, demonstrate that the proposed method dynamically adjusts front and rear axle cornering stiffness, enhancing trajectory tracking accuracy and maneuvering stability, particularly in high-speed or low-friction road conditions.

INDEX TERMS 4WS, trajectory tracking, cornering stiffness estimation, neural network, sliding mode control, fuzzy control.

I. INTRODUCTION

The trajectory tracking capability of a wheeled intelligent fire-fighting robot plays a crucial role in determining its fire-fighting speed. Therefore, the research focus has consistently been on the trajectory tracking control of it. The wheeled fire-fighting robot can be considered as a specialized operational vehicle. Consequently, the research on its trajectory tracking control can still be categorized within the field of vehicle trajectory tracking control. Presently, the global vehicle population is continually increasing, leading to frequent traffic congestion and automobile collisions. The majority of these incidents are closely associated with drivers' poor driving habits [1], [2]. Therefore, the development of advanced driver assistance systems or autonomous driving technologies is deemed crucial to enhance traffic flow efficiency and reduce the occurrence of traffic accidents [3], [4], [5], [6]. In comparison to traditional front-wheel steering vehicles, four-wheel steering (4WS) vehicles offer increased control degrees, providing conditions conducive to enhancing trajectory tracking control accuracy under extreme conditions. Although the application of 4WS technology in conventional fuel-powered vehicles incurs higher costs, the continuous breakthroughs in electric vehicle technology and hub motor technology have significantly lowered its implementation costs. This has rendered the prospects of 4WS technology increasingly promising in various applications [7].

The associate editor coordinating the review of this manuscript and approving it for publication was Xiaosong Hu.

4WS technology can be further classified into two main types based on the control of the rear-wheel steering: Active Rear Wheel Steering (ARS) and Passive Rear Wheel Steering (PRS). In comparison to PRS, ARS can automatically adjust the rear-wheel steering angle according to changes in vehicle speed and driving conditions, significantly enhancing vehicle stability, maneuverability, and cornering performance [8]. Therefore, this work primarily focuses on researching a 4WS control based on ARS. The 4WS trajectory tracking control process can be further decomposed into front wheel trajectory tracking steering control (AFS) and ARS. Currently, various methods have been employed in tra-jectory tracking control research based on AFS, including PID [9], fuzzy logic [10], sliding mode [11], robust control [12], and model predictive control [13]. Among these, the sliding mode control algorithm demonstrates strong adaptability to uncertainties, disturbances, and unmodeled dynamics in control systems, making it particularly suitable for complex environments like vehicle trajectory tracking [14]. Wang and Li [15], using lateral deviation and heading angle deviation as control target quantities, designed two sliding surfaces and developed an intelligent vehicle trajectory tracking controller based on fast reaching law to achieve accurate vehicle trajectory tracking control. Sun et al. [16], aiming to enhance control system robustness, designed an adaptive terminal sliding mode trajectory tracking controller, showing superior control performance under different vehicle speeds and road conditions compared to a regular sliding mode controller. He et al. [17] proposed an inverse sliding mode trajectory tracking controller, which, while actively tracking the reference trajectory, effectively improved the safety and robustness of trajectory tracking. Tagne et al. [18] presented a vehicle lateral displacement control method based on a high-order super-twisting sliding mode controller, which not only ensured convergence of lateral displacement error but also effectively suppressed vibrations near the sliding surface.

Although trajectory tracking control based on sliding mode control algorithms generally performs well in most driving conditions, it still faces challenges in terms of adapt-ability. This is because the vehicle/tire dynamic models used in the field of vehicle control are often simplified, and a single sliding mode control method may struggle to adapt to diverse control requirements. For instance, during actual vehicle operation, factors such as road friction coefficients and the vertical loads borne by each wheel are constantly changing, leading to a strong nonlinear relationship between tire lateral force and slip angle. While a linear cornering stiffness constant can be used when the vehicle is driven with small tire slip angles on a normal road surface, rapid changes in driving conditions often bring the tires close to or even into the nonlinear working range. Adopting a linear cornering stiffness value at such times can result in significant model errors, making it challenging for the controller to ensure the accuracy and stability of vehicle trajectory tracking. Therefore, trajectory tracking controllers designed based on linear cornering stiffness values struggle to meet the requirements of trajectory tracking in complex road conditions. Consequently, many researchers are currently working on integrating various optimization algorithms with sliding mode control algorithms to approximate modeling errors and improve the accuracy and stability of a single sliding mode control method. Kobayashi et al. [19] provided a comprehensive overview of the application of neural networks in autonomous vehicle motion controllers. They proposed the use of radial basis function (RBF) neural networks to approximate unknown disturbances, enhancing the precision and robustness of the control algorithm by establishing a neural network algorithm relating in-puts to unknown disturbances.

Numerous scholars have devoted their efforts to ARS research. Considering the im-pact of road friction coefficient changes on the controller, Zhang et al. [20] introduced variable weighting coefficients for parameter adaptive adjustment to enhance the performance and applicability of the optimal controller. Xie et al. [21] designed an ARS sliding mode con-troller to track the ideal yaw rate, overlooking the fact that the center of gravity lateral deviation is also affected by the rear wheel steering angle. Addressing the limitation of using only yaw rate as a control variable, Qiu et al. [22] proposed a novel structure based on active rear wheel steering to avoid the deterioration of vehicle motion posture during abrupt reverse steering. While the aforementioned ARS control method exhibit good control performance in the vast majority of driving scenarios, achieving satisfactory control effects under extreme driving conditions remains challenging. This is because establishing an accurate mathematical model to represent the vehicle's steering system is highly difficult. Fuzzy control offers advantages such as applicability to nonlinear and complex control systems, independence from control models, and strong resistance to disturbances [23], [24]. Therefore, this work will utilize fuzzy control theory to design the ARS controller.

To this end, this work proposes an 4WS trajectory tracking control method based on time-varying corrected cornering stiffness. A front-wheel steering angle trajectory tracking controller is constructed based on RBF-SMC. In this controller, the cornering stiffness is real-time corrected using the BP cornering stiffness estimation model proposed in this work. The aim is to improve the poor adaptability of the trajectory tracking controller caused by errors in the vehicle/tire dynamic model. Additionally, considering the influence of the center of gravity lateral deviation, a rear-wheel steering angle controller is de-signed based on fuzzy control theory, avoiding the use of the rear-wheel steering system model and addressing the issue of poor control performance due to system modeling errors. In summary, the main contributions of this work can be summarized as follows:

1) Based on the tire magic formula, the nonlinear characteristics of tire lateral force are analyzed, and a cornering stiffness estimation model based on BP neural net-work is proposed.

2) A sliding mode variable structure front-wheel steering trajectory tracking control method is designed, analyzing modeling errors in the sliding mode variable structure control algorithm. The neural network approximation principle is applied to optimize the control method, further reducing lateral errors in the controller.
3) A rear-wheel steering fuzzy control method, taking into account the influence of the center of gravity lateral deviation, is designed. On the basis of eliminating modeling errors in the steering system to improve tracking accuracy, the stability of the vehicle is comprehensively considered.

The rest of this work is organized as follows. In Section II, the method of construction of the cornering stiffness estimation model based on the BP neural network is introduced. In Section III, showing the derivation of the formula for the vehicle trajectory tracking model. In Section IV, the controller for AFS and ARS is designed and integrated into 4WS controllers. In Section V, the 4WS integrated controller performance is validated using the Matlab/Simulink-Carsim co-simulation platform. Conclusions are provided in Section VI.

II. CORNERING STIFFNESS ESTIMATION MODEL

A. NONLINEAR CHARACTERISTICS OF TIRE LATERAL FORCE

The magic formula tire model is the most widely used tire model at present. It is obtained by fitting tire test data with a combination formula of trigonometric functions and accurately describes the nonlinear relationship between tire forces, slip angles, friction coefficients, and slip ratios. The tire lateral force in the magic formula can be expressed as below [25]:

$$f_{yi}(\alpha_i) = d_i \sin\left[c_i \tan^{-1}\left\{b_i(1-e_i)\alpha_i + e_i \tan^{-1}(b_i\alpha_i)\right\}\right] \tag{1}$$

where f_{yi} represents tire lateral force; α_i denotes tire slip angle; b_i, c_i, d_i, and e_i are constant coefficients influenced by tire characteristics, road surface conditions, and vehicle operating conditions. To account for the influence of the friction coefficient μ on lateral force, the coefficients b_i, c_i, and d_i need to be modified to (2-μ)b_i, (5/4-μ/4)c_i, and μd_i.

The influence of vertical load and friction coefficient on tire lateral force is analyzed using the magic formula. As shown in Fig. 1, when the vertical load on the tire varies, the trend of lateral force with respect to slip angle also differs. When the vertical load is 3 kN, the linear lateral force value and nonlinear lateral force value corresponding to a slip angle of 7° are represented by points A and B, respectively, and the discrepancy between them is quite significant. It can be seen from Fig. 2 that when the road friction coefficient changes, the tire lateral force curve exhibits different trends. When the road friction coefficient is 0.5, the linear lateral force value and nonlinear lateral force value corresponding to a slip angle of 7° are represented by points C and D, respectively,

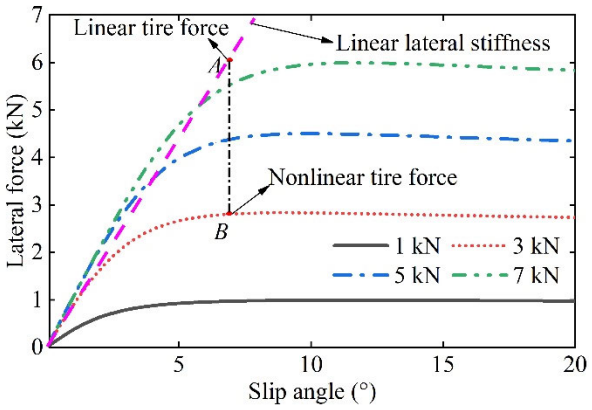

FIGURE 1. Relationship of vertical load and tire lateral force.

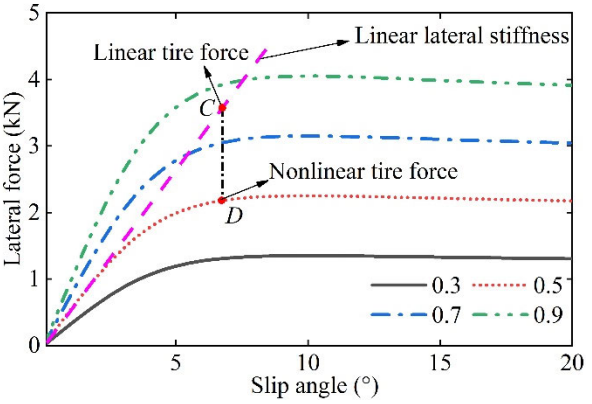

FIGURE 2. Relationship of friction coefficient and tire lateral force.

indicating a significant numerical difference between them. Hence, controllers designed based on linear stiffness calculations for tire forces are unable to adapt to driving conditions where significant changes occur in vertical load and road friction coefficient. Therefore, adaptive adjustments to the cornering stiffness in the controller are necessary based on variables such as vertical load and friction coefficient.

B. ESTIMATION OF CORNERING STIFFNESS BASED ON BP NEURAL NETWORK

1) SELECTION OF ESTIMATION MODEL AND INPUT FEATURES

Tires represent a typical nonlinear system, making it challenging to establish a mathematical expression for the relationship between cornering stiffness and input features using conventional mathematical methods. Neural networks are tools capable of handling nonlinear problems, with BP neural networks being particularly adept at addressing regression problems associated with nonlinear issues. A three-layer BP neural network can approximate any nonlinear equation [26]. Therefore, in this work, a three-layer BP neural network is employed to establish the relationship between cornering stiffness and input features.

The expression for the linear tire model $\breve{f}_{yi}$ is as follows:

$$\breve{f}_{yi} = K_i \alpha_i \tag{2}$$

where K_i represents the linear cornering stiffness. Combining the information from the previous section and (2), it is evident that the primary influencing factors for cornering stiffness are vertical load, friction coefficient, and slip angle. Therefore, these three variables are chosen as input features. Several scholars have proposed methods for estimating road friction coefficient [27] and slip angle [28], thus, these two factors are considered as known quantities in this work. Additionally, vertical load can be obtained through (3) below.

$$\begin{cases} F_{z1} = M \cdot g \dfrac{b}{2(a+b)} - Ma_x \dfrac{h_g}{2(a+b)} - Ma_y \dfrac{h_g}{d} \dfrac{b}{(a+b)} \\ F_{z2} = M \cdot g \dfrac{b}{2(a+b)} - Ma_x \dfrac{h_g}{2(a+b)} + Ma_y \dfrac{h_g}{d} \dfrac{b}{(a+b)} \\ F_{z3} = M \cdot g \dfrac{a}{2(a+b)} + Ma_x \dfrac{h_g}{2(a+b)} - Ma_y \dfrac{h_g}{d} \dfrac{a}{(a+b)} \\ F_{z4} = M \cdot g \dfrac{a}{2(a+b)} + Ma_x \dfrac{h_g}{2(a+b)} + Ma_y \dfrac{h_g}{d} \dfrac{a}{(a+b)} \end{cases} \tag{3}$$

where h_g represents height of the center of gravity, d denotes the wheelbase, g stands for gravitational acceleration, a_x represents longitudinal acceleration, a_y represents lateral acceleration, and a, b represent the distances from the vehicle's center of gravity to the front and rear axles, respectively. The network topology structure of the cornering stiffness estimation model is illustrated in Fig. 3.

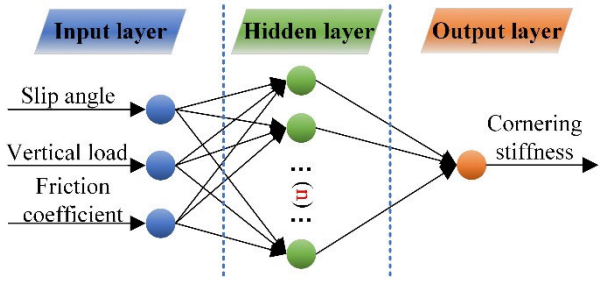

FIGURE 3. Network topology of BP cornering stiffness estimation model.

2) MODEL TRAINING

The training data input matrix as $\boldsymbol{T}_{\text{in}} = [\ \alpha_{\text{in}}\ \boldsymbol{Fz}_{\text{in}} \mu_{\text{in}}]$ is defined, where α_{in}, $\boldsymbol{Fz}_{\text{in}}$, and μ_{in} represent the input matrices for slip angle, vertical load, and friction coefficient. The output matrix is defined as $\boldsymbol{T}_{\text{out}} = C_{\text{out}}$, where $\boldsymbol{C}_{\text{out}}$ is the cornering stiffness output matrix. To reduce numerical disparities among the parameters and enhance estimation accuracy, normalization of the input and output matrices is required. The normalization formula employed in this work is as follows:

$$\chi_{\text{norm}} = \frac{\chi - \chi_{\min}}{\chi_{\max} - \chi_{\min}} \tag{4}$$

where χ represents the value to be normalized, and $\chi_{\min}$ and $\chi_{\max}$ denote the maximum and minimum values in the dataset to be normalized. The expression of the normalized input matrix $\boldsymbol{T}_{\text{innor}}$, after passing through the hidden layer transfer function, can be expressed as:

$$\begin{cases} h_j = \sigma\left(\sum_{i=1}^{\lambda} w_{ij} T_{innor} + \varphi_j\right), (j = 1, 2, \cdots, n) \\ \sigma(\xi) = \dfrac{2}{1 + e^{-2\xi}} - 1 \end{cases} \tag{5}$$

where h_{j} represents the hidden layer output vector, λ denotes the number of input layer nodes, which is 3 in this case, w_{ij} corresponds to the weights from the respective input layer to the hidden layer, φ_j represents the threshold of the hidden layer, $\sigma(\cdot)$ represents the transfer function of the hidden layer, and n represents the number of hidden layer nodes. The range of n is initially determined through empirical formulas, expressed as:

$$n = \sqrt{\kappa + \nu} + \psi \tag{6}$$

where κ represents the number of input layer nodes, ν represents the number of output layer nodes, and ψ is a constant ranging from 0 to 10. The most suitable number of nodes is determined through a trial-and-error approach, with the minimum network error as the measure. The information from hidden layer output nodes is ultimately converged into the output layer nodes, representing the normalized value of cornering stiffness. It can be expressed as:

$$\begin{cases} C_o = \partial\left(\sum_{j=1}^{n} w_{jo} h_j + \tau_o\right), o = 1 \\ \partial(\xi) = \dfrac{1}{1 + e^{-\xi}} \end{cases} \tag{7}$$

where C_o represents the output vector of the output layer, which is the normalized cornering stiffness value. w_{jo} corresponds to the weights between the hidden layer and the output layer, τ_o represents the threshold of the output layer, and $\partial(\cdot)$ represents the activation function of the output layer. The actual output error is calculated based on C_o and compared with the expected output. If the error meets the criteria, the training process stops; otherwise, the weights and thresholds are updated, and the training process is repeated until the error meets the requirements. Finally, the estimative values need to be reverse-normalized to obtain the actual cornering stiffness value. The expression of reverse-normalization χ_{deno} can be expressed as:

$$\chi_{\text{deno}} = \frac{(\chi_{\max} - \chi_{\min})(\chi_{\text{norm}} + 1)}{2} + \chi_{\max} \tag{8}$$

3) TEST SET ESTIMATION RESULTS

In total, 1664 data sets are collected, with 70% used as the training set and 30% as the test set. To provide a clearer presentation of the test results, 127 sets of the test data are randomly selected for result evaluation. As illustrated

in Fig. 4, the curve of actual cornering stiffness values and the estimation curve from the BP model highly coincide, demonstrating a significant alignment. Fig. 5 indicates that the estimation model yields estimation errors within almost 10% for the test set, with a mean estimation error percentage of 2.52%. This result indicates that the proposed cornering stiffness estimation model can provide highly accurate cornering stiffness values for subsequent adaptive trajectory tracking controllers.

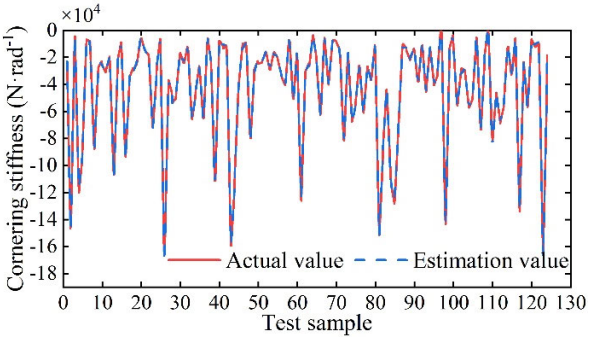

FIGURE 4. Cornering stiffness test set estimation results.

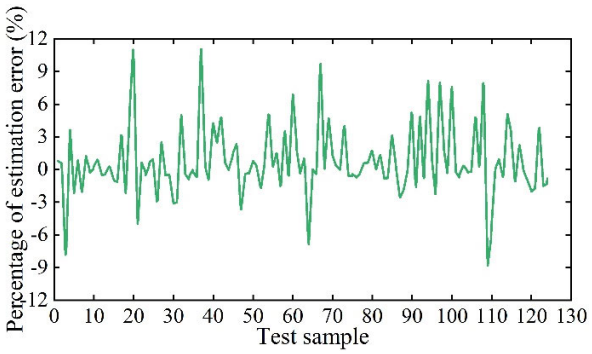

FIGURE 5. Percentage of estimation error of cornering stiffness test set.

III. VEHICLE TRAJECTORY TRACKING MODEL

A. VEHICLE DYNAMICS MODEL

Assuming constant vehicle speed and neglecting the influence of air resistance on the vehicle, the work also ignores the lateral, pitch, and vertical movements of the suspension system. The vehicle dynamics model shown in Fig. 6 is established, which can describe the lateral and yaw dynamic characteristics of the vehicle. In this model, the dynamic coordinate system xoy is fixed on the vehicle body, where the positive x-direction represents the vehicle's forward direction, and the positive y-direction points from the right side to the left side of the vehicle, representing the longitudinal and lateral directions of the vehicle, respectively. In addition, in Fig. 6: u and v represent the longitudinal and lateral velocities of the vehicle, ω_r is the yaw angular velocity, β is the sideslip angle, and δ_f represents the front-wheel steering angle.

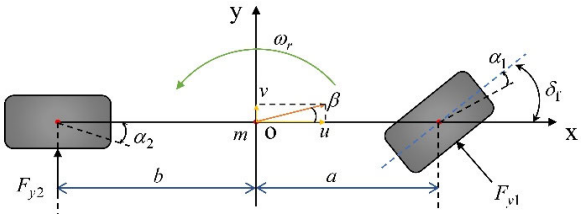

FIGURE 6. Vehicle dynamics model.

The dynamic equations of vehicle can be expressed as follows:

$$\begin{cases} \sum F_y = m\left(\omega_r u + \dot{v}\right) \\ \sum M_z = I_z \dot{\omega}_r \end{cases} \tag{9}$$

where F_y represents the total lateral force at the vehicle's center of mass, M_z denotes the total moment at the vehicle's center of mass, m is the vehicle mass, and I_z denotes the moment of inertia about the z-axis of the vehicle. Assuming a linear relationship between lateral force and slip angle, the two resultant forces in (9) can be expressed as:

$$\begin{cases} \sum F_y = K_1\alpha_1 + K_2\alpha_2 \\ \sum M_z = aK_1\alpha_1 - bK_2\alpha_2 \end{cases} \tag{10}$$

where K_1 and K_2 represent the front and rear tire cornering stiffness, α_1 and α_2 represent the front and rear tire slip angle, respectively, and β represents the sideslip angle. Considering the small values of the sideslip angle β during vehicle motion, α_1 and α_2 can be further expressed as:

$$\begin{cases} \alpha_1 = \beta + a\dfrac{\omega_r}{u} - \delta_1 \\ \alpha_2 = \beta - b\dfrac{\omega_r}{u} \end{cases} \tag{11}$$

Combining (9) to (11), the matrix description of the linear 2-DOF vehicle model can be derived as follows:

$$\begin{bmatrix} \dot{v} \\ \dot{\omega}_r \end{bmatrix} = \begin{bmatrix} \dfrac{K_1+K_2}{mu} & \dfrac{aK_1-bK_2}{mu} - u \\ \dfrac{aK_1-bK_2}{uI_z} & \dfrac{a^2K_1+b^2K_2}{uI_z} \end{bmatrix} \begin{bmatrix} v \\ \omega_r \end{bmatrix} + \begin{bmatrix} -\dfrac{K_1}{m} \\ -\dfrac{aK_1}{I_z} \end{bmatrix} \delta_f \tag{12}$$

B. LATERAL MOTION STATE MODEL

The vehicle tracking model serves as the foundation for studying trajectory tracking, and the tracking error model is one of the commonly used models in intelligent vehicle trajectory tracking. In intelligent vehicle systems, the lateral error and heading angle error between the vehicle and the target trajectory are obtained. These errors are then utilized to adjust the vehicle's operating posture by controlling the accelerator pedal, brake pedal, and steering wheel angle, thereby meeting driving requirements. The trajectory planning incorporates road information, and the lateral error

model is applied to achieve trajectory tracking [29]. Fig. 7 illustrates the vehicle tracking error model.

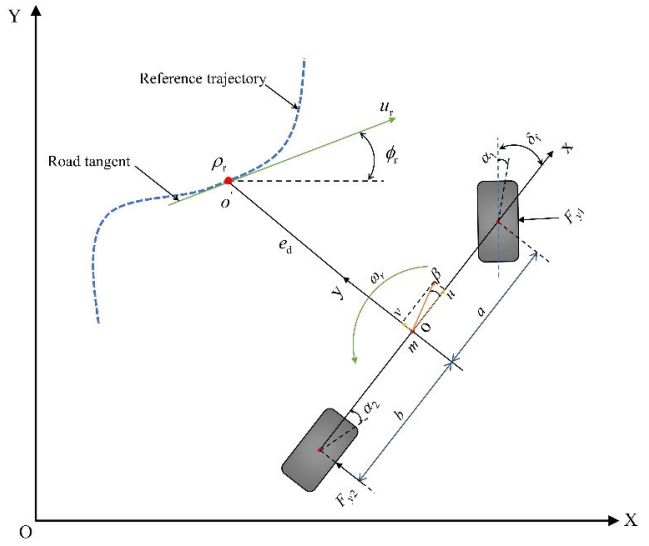

FIGURE 7. Schematic diagram of the vehicle tracking error model.

In Fig. 7, the point o' represents the projection of the vehicle's center of mass on the centerline of the reference path. The lateral error, denoted as e_{d}, is the distance from the vehicle's center of mass to the projection point. At this moment, the heading angle deviation e_ϕ and the road curvature ρ_{r} at the point o' can be expressed as:

$$e_\phi = \phi - \phi_{\mathrm{r}} \tag{13}$$

$$\rho_{\mathrm{r}} = \frac{2\sin(\delta_{\mathrm{f}})}{a+b} \tag{14}$$

where ϕ represents the heading angle of the current vehicle position, ϕ_{r} is the reference heading angle of the vehicle at the time corresponding to the reference trajectory point o'.

At this moment, the vehicle's velocity $\dot{\upsilon}$ at point o' can be defined as:

$$\dot{\upsilon} = \frac{1}{1-\rho_{\mathrm{r}}}\left[u\cos\left(e_\phi\right) - v\sin\left(e_\phi\right)\right] \tag{15}$$

At this juncture, the lateral error and heading angle error of the vehicle can be expressed as:

$$\begin{cases} \dot{e}_d = u\sin\left(e_\phi\right) + v \\ \ddot{e}_d = u\dot{e}_\phi + \dot{v} \\ \dot{e}_\phi = \dot{\phi} - \rho_{\mathrm{r}}\dot{s} \\ \ddot{e}_\phi = \ddot{\phi} \end{cases} \tag{16}$$

Setting $\boldsymbol{e} = \left[e_{\mathrm{d}}\dot{e}_{\mathrm{d}}e_\phi\dot{e}_\phi\right]^{\mathrm{T}}$, the state-space equations for trajectory tracking error can be derived from (13) to (16) as follows:

$$\dot{\boldsymbol{e}} = \boldsymbol{A}\boldsymbol{e} + \boldsymbol{B}\eta + \boldsymbol{C}\phi + \boldsymbol{D} \tag{17}$$

where $\boldsymbol{A}$, $\boldsymbol{B}$, and $\boldsymbol{C}$ can be further expressed as:

$$\boldsymbol{A} = \begin{bmatrix} 0 & 1 & 0 & 0 \\ 0 & a_1 & a_2 & a_3 \\ 0 & 0 & 0 & 1 \\ 0 & a_4 & a_5 & a_6 \end{bmatrix}, \quad \boldsymbol{B} = \begin{bmatrix} 0 \\ b_1 \\ 0 \\ b_2 \end{bmatrix}, \quad \boldsymbol{C} = \begin{bmatrix} 0 \\ c_1 \\ 0 \\ c_2 \end{bmatrix} \tag{18}$$

$\boldsymbol{A}$, $\boldsymbol{B}$, and $\boldsymbol{C}$ are determined by the vehicle's inherent characteristics, where each symbol is defined as follows:

$$\begin{cases} a_1 = \dfrac{(K_1+K_2)}{mu}, a_2 = -\dfrac{(K_1+K_2)}{m}, a_3 = -\dfrac{aK_1 - bK_2}{mu} \\ a_4 = -\dfrac{aK_1 - bK_2}{I_z u}, a_5 = -\dfrac{bK_2 - aK_1}{I_z}, \\ a_6 = -\dfrac{a^2K_1 - b^2K_2}{I_z u} \\ b_1 = -\dfrac{K_1}{m}, b_2 = -\dfrac{aK_1}{I_z}, \ c_1 = \dfrac{aK_1 - bK_2}{mu} - u, \\ c_2 = \dfrac{a^2K_1 + b^2K_2}{I_z u} \end{cases} \tag{19}$$

In accordance with specific driving conditions, the vehicle measures its pose information and reference pose information. Utilizing a control algorithm, the front wheel steering angle and longitudinal vehicle speed are determined to adjust the actual pose of the vehicle. The objective of trajectory tracking is to minimize both lateral distance error and heading angle error, approaching zero, to meet the requirements of planned trajectory tracking.

IV. CONTROLLER DESIGN

The designed four-wheel steering integrated controller with adaptive cornering stiffness (A4WS) primarily consists of an AFS controller and an ARS controller. The logic diagram of the A4WS controller is illustrated in Fig. 8. It is noteworthy that the values K_1 and K_2 in the final solution for δ_{f} should be replaced with the corrected cornering stiffness parameters $\hat{K}_1$ and $\hat{K}_2$ obtained from the cornering stiffness estimation model using BP neural network.

A. AFS CONTROLLER DESIGN

As an inherently highly nonlinear and strongly coupled system, automobiles operate in complex environmental conditions, making them susceptible to influences such as lateral wind and uneven road surfaces during lateral motion [30]. Sliding mode variable structure control, a form of nonlinear control, involves the design of a sliding mode function $u(t)$ and a sliding mode surface $s(t)$. The control principle is to drive a certain spatial state of the controlled system under the action of the sliding mode controller to a pre-designed sliding mode surface. Under the influence of the control law, the points transferred to the sliding mode surface move smoothly on the surface, and the system reaches the origin in finite time. The control is not affected by the inherent parameters of the controlled object. Therefore, sliding mode variable structure

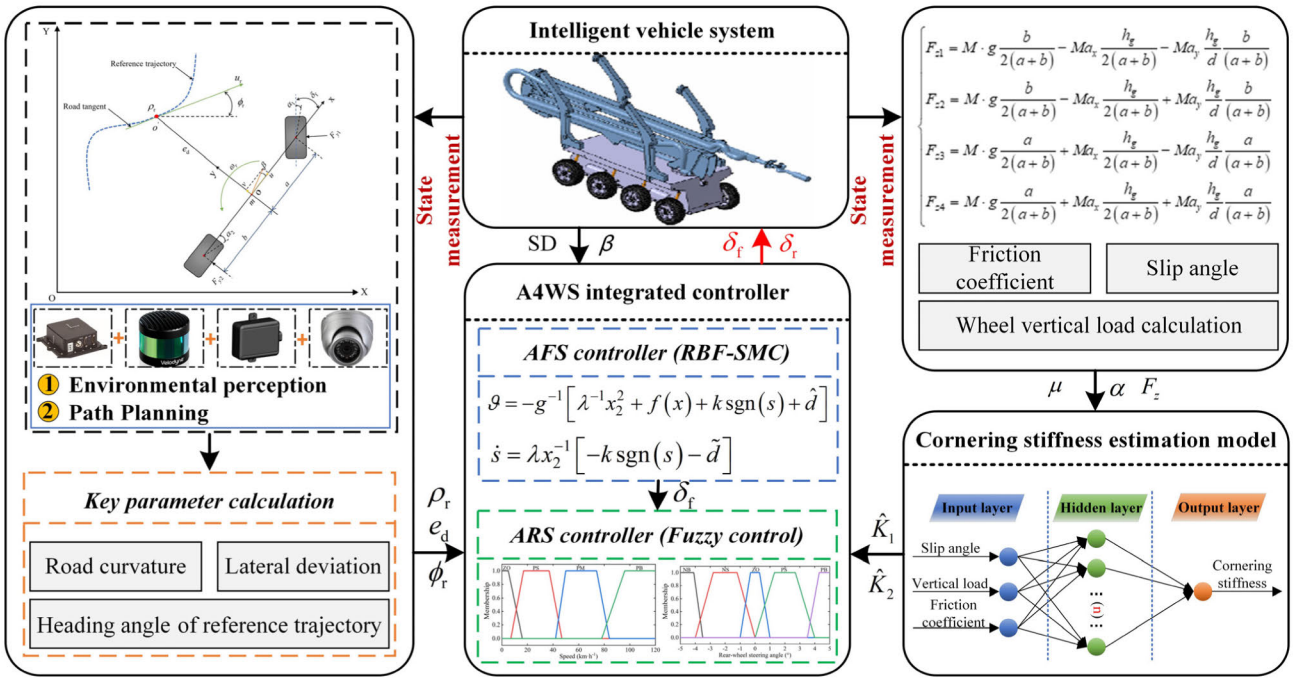

FIGURE 8. A4WS controller logic block diagram.

control exhibits higher robustness compared to other common control systems. Successful implementation of sliding mode variable structure control typically requires the rational design of sliding mode surfaces and sliding mode functions to achieve desirable dynamic performance and robustness [11].

Define a new system error model:

$$x_1 = e_{\mathrm{d}}, \quad x_2 = \dot{e}_{\mathrm{d}} \tag{20}$$

Eliminate lateral error through adjustments to the steering wheel. As defined earlier:

$$\begin{cases} \dot{x}_1 = x_2 \\ \dot{x}_2 = f\left(x\right) + g\left(x\right)\eta + d_t \end{cases} \tag{21}$$

where d_t represents the unknown disturbance term in vehicle trajectory tracking. As deduced from the dynamic equations derived in the preceding section:

$$\begin{cases} f\left(x\right) = a_1\dot{e}_{\mathrm{d}} + a_2 e_\phi + a_{3e}\dot{e}_\phi + c_1\phi \\ g\left(x\right) = b_1 \end{cases} \tag{22}$$

The primary objective of trajectory tracking is to eliminate lateral error and heading angle error to achieve tracking of the desired trajectory. Therefore, the sliding surface function can be defined as:

$$s = x_1 + \lambda x_2 \tag{23}$$

where λ represents the sliding surface coefficient. The sliding mode motion comprises two processes: the approaching motion and the sliding motion. Employing an approaching law can enhance the dynamic performance of the approaching motion. To ensure rapid convergence while mitigating chattering, an exponential approaching law is selected, expressed as:

$$\dot{s} = -ksgn\left(s\right), \quad k > 0 \tag{24}$$

where k represents the approaching law coefficient. To ensure that the system moves on the sliding mode surface, it is necessary to satisfy the stability conditions of the system. As derived from (22) and (23), along with the approaching law, the output of the vehicle's front wheel steering angle can be expressed as:

$$\delta_{\mathrm{f}} = -g^{-1}\left[\lambda^{-1}x_2^2 + f\left(x\right) + ksgn\left(s\right) + d\left(t\right)\right] \tag{25}$$

The neural network-based sliding mode variable structure algorithm can directly output control signals based on lateral error and heading angle deviation state information. It can also serve as vehicle state parameters, optimizing parameters for other control algorithms to enhance control precision. Consequently, it can approximate unknown modeling errors and external disturbances, improving the robustness and control accuracy of intelligent vehicle lateral control strategies [31]. Regarding the sum of unknown errors and modeling errors, denoted as d_t, it profoundly affects the accuracy of vehicle lateral tracking. By minimizing the impact of d_t on lateral error, the controller achieves a relatively high level of precision. The RBF neural network algorithm possesses strong nonlinear fitting capabilities, constituting a three-layer feedforward network with simple learning rules and rapid convergence. It is commonly employed to optimize parameters for other control algorithms, enhancing algorithm

precision [32]. The input-output algorithm for the RBF network is expressed as:

$$h_j = \exp\left(\frac{\|\boldsymbol{x} - \boldsymbol{c}_j\|}{2b_j^2}\right) \tag{26}$$

$$f = \boldsymbol{W}^{*\mathrm{T}}\boldsymbol{h}(\boldsymbol{x}) + \varepsilon \tag{27}$$

where x represents the grid input, j denotes the j-th grid input in the hidden layer of the network, $\boldsymbol{h}=[h_j]^{\mathrm{T}}$ represents the output of the Gaussian basis function, $\boldsymbol{W}^*$ is the ideal network weight, ε is the network approximation error with $\varepsilon \leq \varepsilon_{\mathrm{N}}$, f is the grid output. When the grid input is set to $x = [e_{\mathrm{d}}\dot{e}_{\mathrm{d}}]^{\mathrm{T}}$, the control law is given by:

$$\vartheta = -g^{-1}\left[\lambda^{-1}x_2^2 + f(x) + ksgn(s) + \hat{d}\right] \tag{28}$$

Substituting the new control law (28) into (23) yields:

$$\dot{s} = \lambda x_2^{-1}\left[-ksgn(s) - \tilde{d}\right] \tag{29}$$

where, let $\tilde{d}(t) = \tilde{\boldsymbol{W}}^{\mathrm{T}}\boldsymbol{h}(\boldsymbol{x}) + \varepsilon$, $\tilde{\boldsymbol{W}} = \hat{\boldsymbol{W}} - \boldsymbol{W}$.

Define the Lyapunov function as:

$$L = \frac{1}{2}s^2 + \frac{1}{2}\varsigma\tilde{\boldsymbol{W}}\tilde{\boldsymbol{W}}^{\mathrm{T}} \tag{30}$$

where, $\varsigma > 0$. Choosing the adaptive law $\dot{\hat{W}} = \frac{1}{\varsigma}h(x)s\lambda$, the expression can be obtained:

$$\dot{L} = s\lambda x_2^{-1}(-ksgn(s) - \varepsilon) \tag{31}$$

As the approximation error can be sufficiently constrained, it can be deduced that $\dot{L} \leq 0$. Therefore, the sliding mode control system based on neural networks is stable. In other words, under the optimization of the neural network for the sliding mode control strategy, the front wheel steering angle output can still reach the desired state.

B. ARS CONTROLLER DESIGN

The primary structure of the fuzzy control strategy for rear-wheel steering utilizes vehicle speed (SD), front-wheel steering angle, and center of gravity lateral deviation as input parameters, with rear-wheel steering angle as the output, as illustrated in Fig. 9.

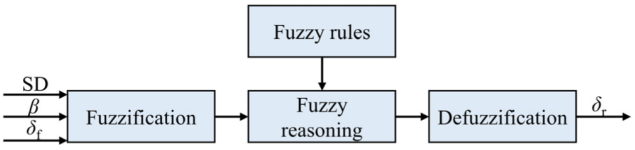

FIGURE 9. Block diagram of the rear-wheel steering fuzzy controller structure.

1) DEFINE THE VARIABLES

The typical speed of a vehicle during normal operation generally does not exceed 120 km/h. Therefore, the selected speed range is [0, 120], divided into four intervals: {Zero, Low, Medium, High}, denoted as {ZO, PS, PM, PB}. The mechanical design range for the front-wheel steering angle is usually −25° to 25°. Hence, the defined range for the front-wheel steering angle is [−25, 25], subdivided into five intervals: {Negative Large, Negative Small, Zero, Positive Small, Positive Large}, denoted as {NB, NS, ZO, PS, PB}. The boundary of the center of gravity lateral deviation is directly related to the road friction coefficient. The condition producing the maximum center of gravity lateral deviation is when the road has the maximum friction force. The sign of the center of gravity lateral deviation is related to the vehicle's direction. To simplify the complexity of fuzzy rules, the input center of gravity lateral deviation is taken as its absolute value. Thus, the defined range for the center of gravity lateral deviation is [0, 10], divided into four intervals: {Zero, Low, Medium, High}, denoted as {ZO, PS, PM, PB}. As this work focuses on high-speed limit conditions, when the speed is greater than 35 km/h, the rear-wheel steering direction aligns with the front wheels and does not exceed 5° [33]. Therefore, the defined range for the rear-wheel steering angle is [−5 5], subdivided into five intervals: {Negative Large, Negative Small, Zero, Positive Small, Positive Large}, denoted as {NB, NS, ZO, PS, PB}.

2) FUZZIFICATION

After analyzing the characteristics of each membership function, a trapezoidal membership function curve is selected, as illustrated in Fig. 10.

3) DEVELOPMENT OF FUZZY RULES AND DEFUZZIFICATION

The 4WS vehicle possesses the advantages of high maneuverability in low-speed working modes and stability in high-speed working modes. Therefore, in low-speed turning conditions, to enhance the vehicle's agility, an inverse-phase control mode with opposite steering directions of the front and rear wheels is adopted, resulting in larger rear-wheel steering angles. In extreme conditions, to ensure the stability of the vehicle during turns, the front and rear wheels adopt an in-phase control mode with the same steering directions, outputting larger rear-wheel steering angles. Ultimately, fuzzy rear-wheel steering angle parameters are obtained. The specific fuzzy rules are presented in Table 1. In this study, the commonly used center of gravity method is chosen for defuzzification. Fuzzy inference is performed based on the formulated fuzzy rules, and then, through defuzzification, the corresponding rear-wheel steering angle value δ_{r} can be determined.

V. DISCUSSION AND ANALYSIS OF SIMULATION RESULTS

To validate the superiority of the proposed 4WS trajectory tracking controller, a comparative study is conducted using the Matlab/Simulink-Carsim co-simulation platform. A comparison is made with a 4WS trajectory tracking controller employing constant cornering stiffness. The vehicle parameters involved are presented in Table 2. Three simulated test scenarios are designed based on the vehicle's typical driving conditions in this work. Test scenario 1: The road surface is

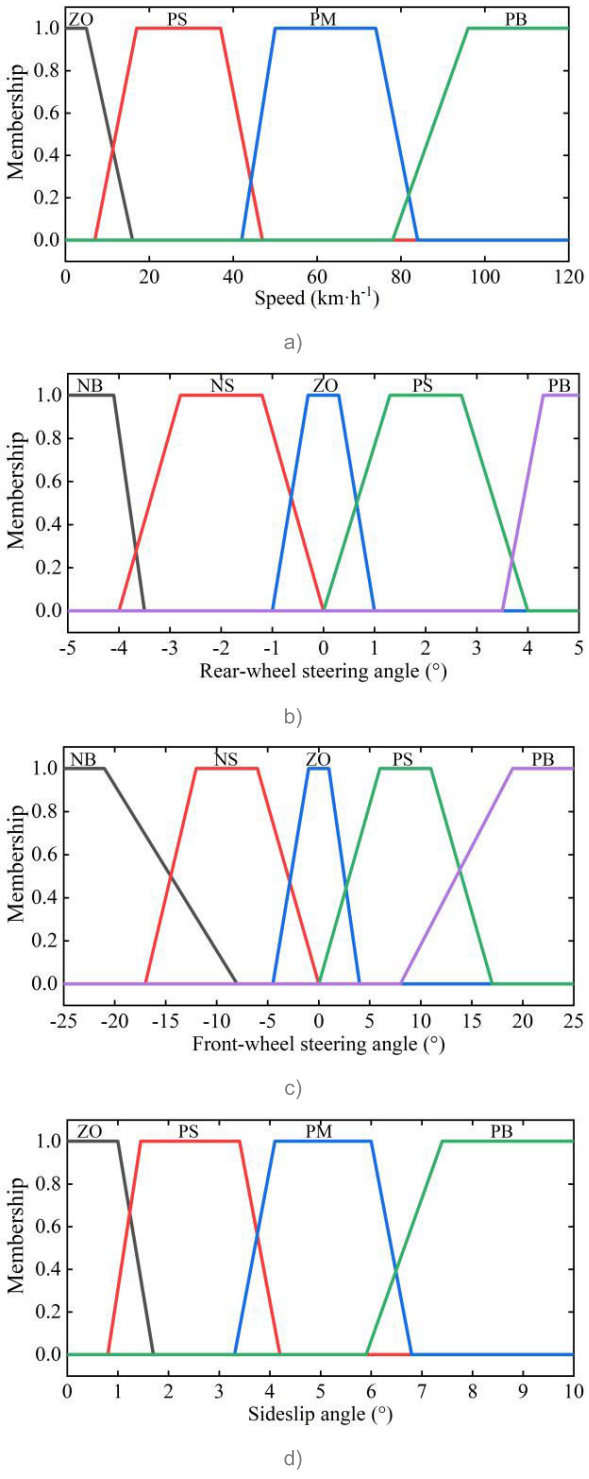

FIGURE 10. Membership Function Curves: a) Speed, b) Rear-wheel steering angle, c) Front-wheel steering angle, and d) Sideslip angle.

covered with ice and snow, with a road friction coefficient of approximately 0.3, and the vehicle speed is set at 60 km/h. Test scenario 2: The road surface is dry asphalt, with a friction coefficient of around 0.8, and the vehicle speed is maintained at 60 km/h. Test scenario 3: The road surface remained dry asphalt, but the vehicle speed is increased to 100 km/h.

TABLE 1. Fuzzy rule control table.

Speed	Sideslip angle	Front-wheel steering angle				
		NB	NS	ZO	PS	PB
ZO	ZO	ZO	ZO	ZO	ZO	ZO
	PS	ZO	ZO	ZO	ZO	ZO
	PM	ZO	ZO	ZO	ZO	ZO
	PB	ZO	ZO	ZO	ZO	ZO
PS	ZO	PB	PS	ZO	NS	NB
	PS	PB	PS	ZO	NS	NB
	PM	NS	NS	ZO	PS	PS
	PB	NB	NS	ZO	PS	PB
PM	ZO	NS	NS	ZO	PS	PS
	PS	NS	NS	ZO	PS	PS
	PM	NB	NS	ZO	PS	PB
	PB	NB	NB	ZO	PB	PB
PB	ZO	NB	NS	ZO	PS	PB
	PS	NB	NS	ZO	PS	PB
	PM	NB	NS	ZO	PS	PB
	PB	NB	NB	ZO	PB	PB

TABLE 2. Vehicle parameters.

Vehicle parameter name	Value
m	1412 kg
a	1.015 m
b	1.895 m
K_1	-149161 N • rad^{-1}
K_2	-89624 N • rad^{-1}
I_z	1536.7 kg • m^2

This work primarily focuses on the trajectory tracking control performance of the designed controller. Therefore, the path planning component is not considered. Instead, an existing trajectory model is directly chosen as the reference trajectory, expressed as follows [15]:

$$\begin{cases} y_o(x) = \dfrac{p_1}{2}\left[1+\tanh(\gamma_1)\right] - \dfrac{p_2}{2}\left[1+\tanh(\gamma_2)\right] \\ \sigma_o(x) = \arctan\left[\begin{array}{c} p_1\left(\frac{1}{\cosh(\gamma_1)}\right)^2\left(\frac{1.2}{\tau_1}\right) \\ -p_2\left(\frac{1}{\cosh(\gamma_2)}\right)^2\left(\frac{1.2}{\tau_2}\right) \end{array}\right] \end{cases} \tag{32}$$

where y_o is the reference value for the lateral position of the vehicle during driving, and x is the reference value for the longitudinal position, σ_o is the heading angle reference value. Taking $\gamma_1 = 0.096(x\text{-}60)\text{-}1.2$, $\gamma_2 = 0.096(x\text{-}120)\text{-}1.2$, $\tau_1 = \tau_2 = 25$ and $p_1 = p_2 = 3.5$.

A. TEST SCENARIO 1: LOW SPEED ICE AND SNOW ROAD

It can be seen from Fig. 11 that under the low-speed icy road conditions, the proposed A4WS controller enables the vehicle to achieve higher tracking accuracy. As depicted in Fig. 12, the maximum lateral deviation obtained with the 4WS controller is 0.2441 m, while with the A4WS controller, the maximum lateral deviation is reduced to0.1607 m, a reduction of 34.17%. Fig. 13 reveals that the maximum yaw rate based on the A4WS controller is 0.2309 rad·s^{-1}, compared to 0.2605 rad·s^{-1} with the 4WS controller, indicating a decrease of 11.36% in the maximum yaw rate.

Fig. 14 shows the real-time estimation of the front and rear axle cornering stiffness by the BP cornering stiffness

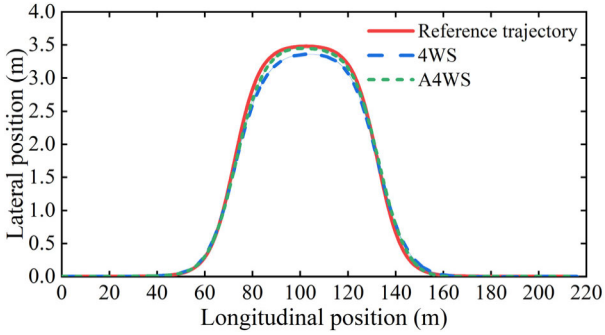

FIGURE 11. Lateral displacement under test scenario 1.

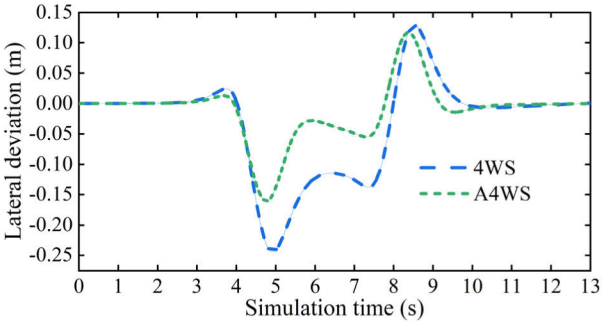

FIGURE 12. Lateral deviation under test scenario 1.

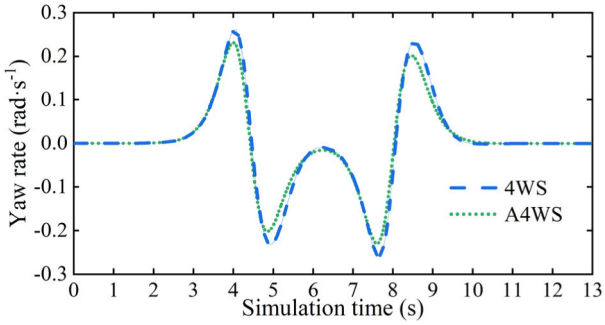

FIGURE 13. Yaw rate under test scenario 1.

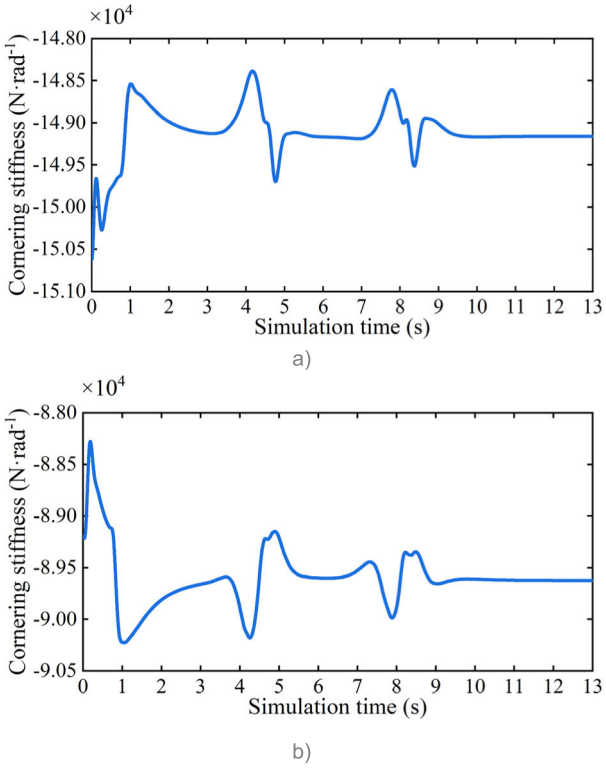

FIGURE 14. Cornering stiffness under test scenario 1: a) Front axle, and b) Rear axle.

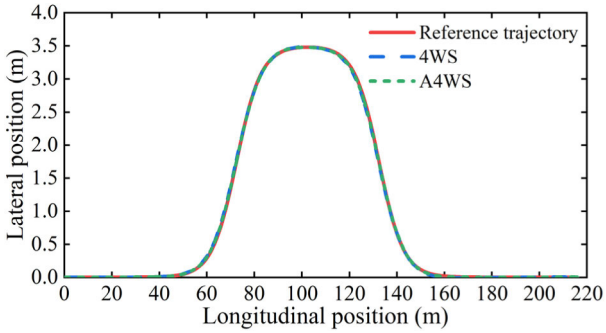

FIGURE 15. Lateral displacement under test scenario 2.

estimator under test scenario 1. From this figure, it can be seen that the two main correction points are at the two inflection points of the double shift peak, at which point the tire nonlinearity is strongest. It is worth noting that both cornering stiffness correction curves exhibited significant fluctuations at the beginning. This might be attributed to the initial longitudinal speed control fluctuations, leading to vertical load transfer between the front and rear wheels. In this scenario, the A4WS controller not only enhances trajectory tracking accuracy but also exhibits a faster convergence response of the yaw rate to its steady-state value.

B. TEST SCENARIO 2: LOW SPEED DRY ASPHALT ROAD

It can be seen from Fig. 15 that under the low-speed dry asphalt road conditions, both the proposed A4WS controller and the 4WS controller demonstrate a high level of tracking accuracy. As shown in Fig. 16, the maximum lateral deviation obtained with the 4WS controller is 0.0584 m, while with the A4WS controller, the maximum lateral deviation is reduced to 0.0277 m, a reduction of 52.57%. Fig. 17 indicates that the maximum yaw rate achieved with the 4WS controller is 0.2143 rad·s^{-1}, whereas with the A4WS controller, the maximum yaw rate is 0.2098 rad·s^{-1}, both being relatively small.

Fig. 18 shows the real-time estimated front and rear axle cornering stiffness by the BP cornering stiffness estimator under test scenario 2. Compared to test scenario 1, the amplitude of the cornering stiffness correction curve fluctuations is smaller. This is because the road conditions are better, increasing the threshold for tire entry into the nonlinear working range. Under this scenario, the A4WS controller and the 4WS controller exhibit similar control effectiveness.

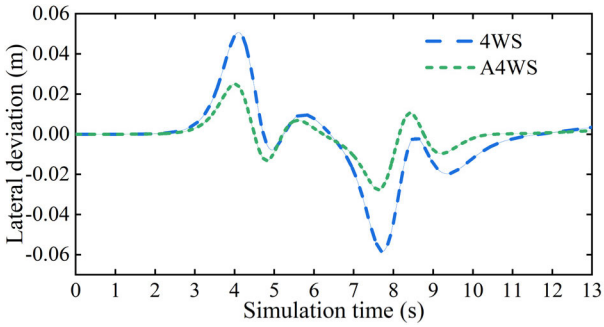

FIGURE 16. Lateral deviation under test scenario 2.

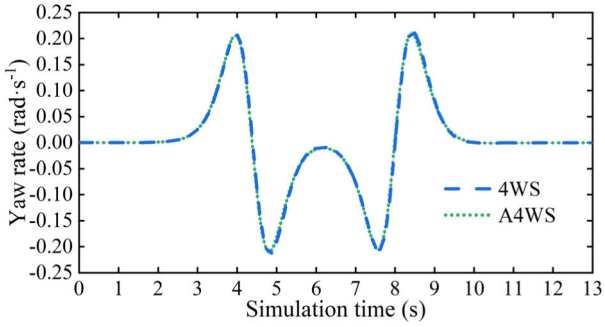

FIGURE 17. Yaw rate under test scenario 2.

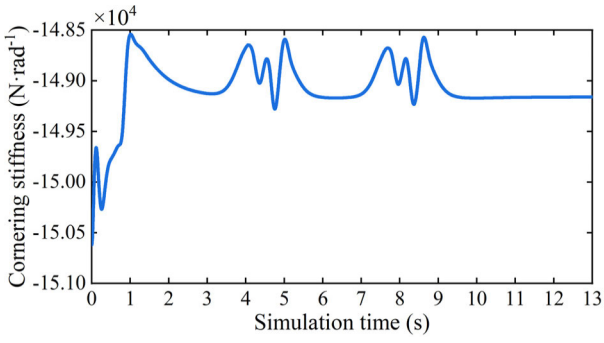

FIGURE 18. Cornering stiffness under test scenario 2: a) Front axle, and b) Rear axle.

C. TEST SCENARIO 3: HIGH SPEED DRY ASPHALT ROAD

It can be seen from Fig. 19 that under high-speed dry asphalt road conditions, both the proposed A4WS controller and the 4WS controller exhibit noticeable deviations when the

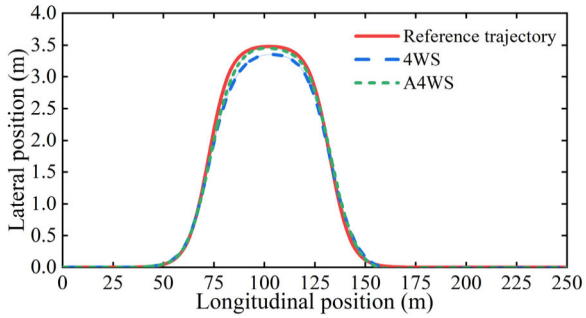

FIGURE 19. Lateral displacement under test scenario 3.

lateral distance from the reference trajectory is at its maximum. As shown in Fig. 20, the maximum lateral deviation obtained with the 4WS controller is 0.2937 m, while with the A4WS controller, the maximum lateral deviation is reduced to 0.1961 m, a reduction of 33.23%. Fig. 21 demonstrates that the maximum yaw rate achieved with the 4WS controller is 0.4338 rad·s^{-1}, whereas with the A4WS controller, the maximum yaw rate is reduced to 0.3750 rad·s^{-1}, a decrease of 13.55%.

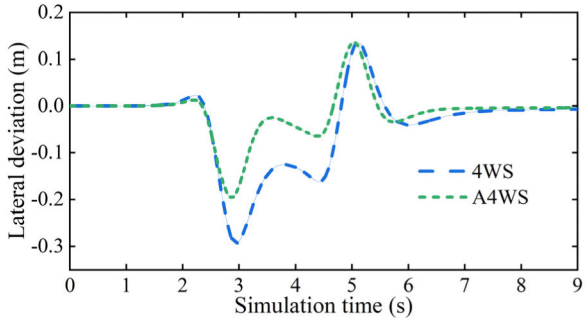

FIGURE 20. Lateral deviation under test scenario 3.

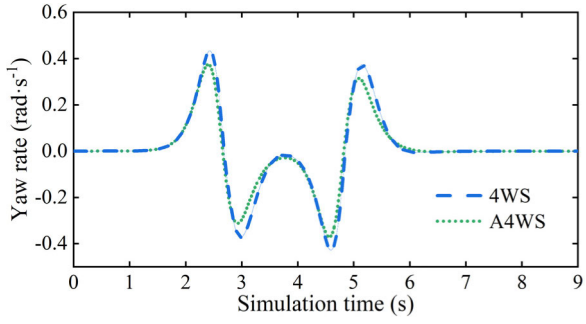

FIGURE 21. Yaw rate under test scenario 3.

Fig. 22 presents the real-time estimated front and rear axle lateral stiffness by the BP cornering stiffness estimator under test scenario 3. Compared to test scenario 2, the amplitude of the cornering stiffness correction curve fluctuations significantly increases. This is because the increase in vehicle speed further enhances the tire's nonlinearity during steering,

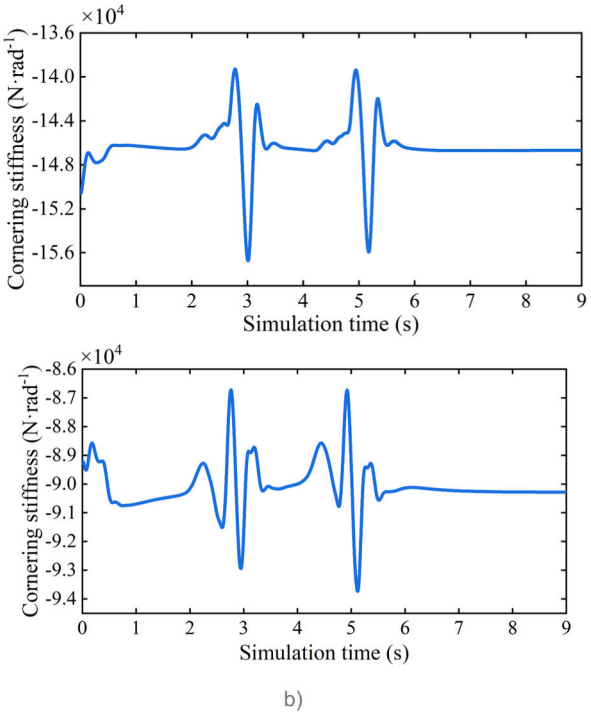

FIGURE 22. Cornering stiffness under test scenario 3: a) Front axle, and b) Rear axle.

enlarging the error between linear tire force and actual tire force. Under this scenario, the A4WS controller with variable cornering stiffness correction ensures both tracking the reference trajectory and maintaining excellent vehicle handling stability.

VI. CONCLUSION

This work proposes a trajectory tracking control method for 4WS intelligent vehicles that takes into consideration the adaptive cornering stiffness of tires. This method aims to enhance the accuracy and operational adaptability of vehicle trajectory tracking, particularly in extreme driving conditions. The main conclusions are summarized as follows:

1) The influence of vertical load and road friction coefficient on the nonlinear characteristics of tire lateral forces is analyzed based on the magic formula. A tire cornering stiffness estimation model is established using a BP neural network. Test results indicated that the established tire cornering stiffness estimation model has an estimation mean deviation within 10% for the test set, with a mean estimation error percentage of 2.52%.
2) Based on the 2-DOF vehicle dynamics model and the trajectory tracking error model, the state equations for trajectory tracking are established. A trajectory tracking sliding mode controller for active front-wheel steering is designed. Additionally, an RBF is employed to further optimize system errors, creating an RBF-SMC AFS controller capable of real-time correction of cornering stiffness. Considering the impact of the center of gravity lateral deviation on vehicle stability, a fuzzy controller for ARS is designed. The integration of the AFS controller and the ARS fuzzy controller resulted in the development of the A4WS integrated controller.
3) A co-simulation model is established using Carsim and Matlab/Simulink. Simulation results indicate that, compared to the 4WS controller, the intelligent vehicle based on the A4WS controller can dynamically adjust the front and rear axle cornering stiffness according to driving conditions in real-time. This adjustment significantly enhances the precision of vehicle trajectory tracking and handling stability. Particularly, it proves valuable for enhancing the adaptability of intelligent vehicle control systems, especially at high speeds or low road friction conditions.

REFERENCES

[1] H. Wang, Y. Huang, A. Khajepour, D. Cao, and C. Lv, "Ethical decision-making platform in autonomous vehicles with lexicographic optimization based model predictive controller," *IEEE Trans. Veh. Technol.*, vol. 69, no. 8, pp. 8164–8175, Aug. 2020.

[2] J. Davins-Valldaura, F. Plestan, S. Moussaoui, and G. Pita-Gil, "Design and optimization of nonlinear observers for road curvature and state estimation in automated vehicles," *IEEE Trans. Intell. Transp. Syst.*, vol. 18, no. 12, pp. 3315–3327, Dec. 2017.

[3] P. Zhang, Y. Chen, S. Jiang, and Y. Han, "Trajectory planning and tracking control of automatic overtaking process on highway," *J. Automot. Saf. Energy*, vol. 13, no. 3, pp. 463–472, May 2022.

[4] Y. Zang, Y. Cai, X. Sun, X. Xu, L. Chen, and H. Wang, "Research on intelligent vehicle trajectory tracking coordination control method based on extension game," *J. Mech. Eng., Chin. Ed.*, vol. 58, no. 8, pp. 181–194, Apr. 2022.

[5] J. Ji, A. Khajepour, W. W. Melek, and Y. Huang, "Path planning and tracking for vehicle collision avoidance based on model predictive control with multiconstraints," *IEEE Trans. Veh. Technol.*, vol. 66, no. 2, pp. 952–964, Feb. 2017.

[6] Y. Huang, H. Ding, Y. Zhang, H. Wang, D. Cao, N. Xu, and C. Hu, "A motion planning and tracking framework for autonomous vehicles based on artificial potential field elaborated resistance network approach," *IEEE Trans. Ind. Electron.*, vol. 67, no. 2, pp. 1376–1386, Feb. 2020.

[7] H. Wei, "Research on four-wheel steering control strategy based on electric wheel vehicle," *Agricult. Equip. Vehicle Eng.*, vol. 61, no. 7, pp. 120–124, Feb. 2023.

[8] P. Hang and X. Chen, "Path tracking control of 4-wheel-steering autonomous ground vehicles based on linear parameter-varying system with experimental verification," *Proc. Inst. Mech. Eng., I, J. Syst. Control Eng.*, vol. 235, no. 3, pp. 411–423, Mar. 2021.

[9] R. Marino, S. Scalzi, and M. Netto, "Nested PID steering control for lane keeping in autonomous vehicles," *Control Eng. Pract.*, vol. 19, no. 12, pp. 1459–1467, Dec. 2011.

[10] A.-T. Nguyen, C. Sentouh, H. Zhang, and J.-C. Popieul, "Fuzzy static output feedback control for path following of autonomous vehicles with transient performance improvements," *IEEE Trans. Intell. Transp. Syst.*, vol. 21, no. 7, pp. 3069–3079, Jul. 2020.

[11] C. Hu, R. Wang, and F. Yan, "Integral sliding mode-based composite nonlinear feedback control for path following of four-wheel independently actuated autonomous vehicles," *IEEE Trans. Transport. Electrific.*, vol. 2, no. 2, pp. 221–230, Jun. 2016.

[12] J. Guo, Y. Luo, K. Li, and Y. Dai, "Coordinated path-following and direct yaw-moment control of autonomous electric vehicles with sideslip angle estimation," *Mech. Syst. Signal Process.*, vol. 105, pp. 183–199, May 2018.

[13] R. Du, H. Hu, K. Gao, and H. Huang, "Research on trajectory tracking control of autonomous vehicle based on MPC with variable predictive horizon," *J. Mech. Eng., Chin. Ed.*, vol. 58, no. 24, pp. 275–288, Aug. 2022.

[14] T. Chen, X. Xu, Y. Cai, and X. Sun, "Coordinated control of front-wheel steering angle and yaw stability for unmanned ground vehicle based on state estimation," *Trans. Beijing Inst. Tech.*, vol. 41, no. 10, pp. 1050–1057, May 2021.
[15] J. Wang and J. Li, "Research on coordinated control of trajectory tracking and yaw stability of unmanned ground vehicle," *J. Chongqing Univ. Technol., Nat. Sci.*, vol. 35, no. 7, pp. 62–70, Feb. 2021.
[16] Z. Sun, J. Zou, J. Pan, and D. He, "Path tracking control for autonomous vehicles using adaptive integral terminal sliding mode," *J. Zhejiang Univ. Technol.*, vol. 49, no. 5, pp. 494–502, Aug. 2021.
[17] X. He, Y. Liu, C. Lv, X. Ji, and Y. Liu, "Emergency steering control of autonomous vehicle for collision avoidance and stabilisation," *Vehicle Syst. Dyn.*, vol. 57, no. 8, pp. 1163–1187, Aug. 2019.
[18] G. Tagne, R. Talj, and A. Charara, "Higher-order sliding mode control for lateral dynamics of autonomous vehicles, with experimental validation," in *Proc. IEEE Intell. Vehicles Symp. (IV)*, 2013, pp. 678–683.
[19] T. Kobayashi, E. Katsuyama, H. Sugiura, Y. Hattori, E. Ono, and M. Yamamoto, "Theoretical analysis of tyre slip power dissipation mechanism using brush model," *Vehicle Syst. Dyn.*, vol. 58, no. 8, pp. 1242–1256, Aug. 2020.
[20] S. Zhang, H. Wang, P. Chen, X. Zhang, and Q. Li, "A review of the application of neural networks in motion control of unmanned vehicles," *Chin. J. Eng.*, vol. 44, no. 2, pp. 235–243, Apr. 2022.
[21] X. Xie, L. Jin, L. Gao, and H. Xia, "Research on LQR vehicle rear-wheel active steering control based on variable weight coefficient," *J. Zhejiang Univ., Eng. Sci.*, vol. 52, no. 3, pp. 446–452, May 2018.
[22] H. Qiu, Z. Dong, and Z. Lei, "Integrated control and test of four-wheel independent drive electric vehicle ARS and DYC," *J. Jiangsu Univ., Nat. Sci.*, vol. 37, no. 3, pp. 268–276, Apr. 2016.
[23] S. Wagner, T. Weiskircher, D. Ammon, and G. Prokop, "Pivot point-based control for active rear-wheel steering in passenger vehicles," *Vehicle Syst. Dyn.*, vol. 56, no. 8, pp. 1139–1161, Aug. 2018.
[24] Y. Cao and M. Qiao, "Research on rear wheel Angle fuzzy controller of four-wheel steering vehicle," *Mech. Des. Manuf.*, vol. 6, pp. 66–73, May 2020.
[25] S. Mammar and D. Koenig, "Vehicle handling improvement by active steering," *Vehicle Syst. Dyn.*, vol. 38, no. 3, pp. 211–242, Sep. 2002.
[26] B. Li, Z. Quan, S. Bei, L. Zhang, and H. Mao, "An estimation algorithm for tire wear using intelligent tire concept," *Proc. Inst. Mech. Engineers, D, J. Automobile Eng.*, vol. 235, nos. 10–11, pp. 2712–2725, Feb. 2021.
[27] B. Zhu, J. Piao, J. Zhao, J. Wu, and W. Deng, "Vehicle longitudinal collision warning strategy based on road adhesion coefficient estimation," *Automot. Eng.*, vol. 38, no. 4, pp. 446–452, Apr. 2016.
[28] X. Zhang, B. Chen, J. Song, and Q. Wang, "Research on measuring method of automobile tire slip angle under extreme working condition," *Trans. Chin. Soc. Agric. Mach.*, vol. 45, no. 9, pp. 34–36, May 2014.
[29] L. Xiong, X. Yang, G. Zhuo, B. Leng, and R. Zhang, "Review on motion control of autonomous vehicles," *J. Mech. Eng., Chin. Ed.*, vol. 56, no. 10, pp. 127–143, Aug. 2020.
[30] K. Liu, H. Chen, J. Gong, S. Chen, and Y. Zhang, "Research on the handling stability of high-speed unmanned vehicles," *Automot. Eng.*, vol. 41, no. 5, pp. 514–521, Jun. 2019.
[31] W. Zhao and H. Zhang, "Coupling control strategy of force and displacement for electric differential power steering system of electric vehicle with motorized wheels," *IEEE Trans. Veh. Technol.*, vol. 67, no. 9, pp. 8118–8128, Sep. 2018.
[32] W. Zhang, H. Han, Y. Yang, and Y. Yi, "Neural network driverless control based on driver behavior," *J. South China Univ. Technol., Nat. Sci.*, vol. 44, no. 12, pp. 74–80, Jun. 2016.
[33] S. Dupond, "A thorough review on the current advance of neural network structures," *Annu. Rev. Control.*, vol. 14, no. 14, pp. 200–230, Jul. 2019.
[34] L. Zhang, H. Ding, K. Guo, J. Zhang, W. Pan, and Z. Jiang, "Cooperative chassis control system of electric vehicles for agility and stability improvements," *IET Intell. Transp. Syst.*, vol. 13, no. 1, pp. 134–140, Nov. 2018.

LIN ZHONG is currently an Associate Research Fellow with Shanghai Fire Research Institute, Ministry of Emergency Management, mainly engaged in fire robot, fire boat equipment key technology research, and related inspection and testing technology research. She is also a Professional Degree Tutor with the School of Mechanical and Vehicle Engineering, Hunan University, and a Master's Tutor with Xi'an University of Science and Technology.

XUDONG JIANG is currently a Research Fellow with Shanghai Fire Research Institute, Ministry of Emergency Management, mainly engaged in fire control vehicles and equipment inspection and research.

WENLONG JIA is currently a Research Associate with Shanghai Fire Research Institute, Ministry of Emergency Management, mainly engaged in the research of fire robots and fire boat inspection and testing technology.

WEI SHI is currently an Associate Research Fellow with Shanghai Fire Research Institute, Ministry of Emergency Management, mainly engaged in the research of key technology of fire equipment and autonomous control technology of fire robot.